Recombination and impact-ionization peculiarities in many-valley semiconductors

V. V. Mitin*

Max-Planck-Institut für Festkörperforschung, D-7000 Stuttgart 80, West Germany

M. Asche and H. Kostial

*Zentralinstitut für Elektronenphysik der Akademie der Wissenschaften der Deutsches Demokratisches Republik,
DDR-1086 Berlin, Germany*

Investigations were performed for n-type Si at 27 K in the presence of heating electric and strong magnetic fields taking the anisotropy of the effective mass and additionally of the carrier scattering time on acoustic phonons properly into account. This consideration of the many-valley band structure and the consequent intervalley repopulation yields very significant dependences of mean carrier velocities, recombination at shallow donors, as well as their impact-ionization and intervalley scattering times on the orientations of the applied fields. The calculated change of the carrier concentration with heating exhibits N- and S-type behavior for certain field orientations, and the numerically obtained current-voltage characteristics in the absence and presence of magnetic fields agree well with the experimentally determined ones.

I. INTRODUCTION

The capture of hot carriers by attractive centers and the impact ionization of neutral centers were most frequently investigated in n-type Ge (Refs. 1—5) and n-type Si (Refs. 6 and 7), i.e., in many-valley semiconductors. Therefore it is expected that the orientation of the heating field with respect to the equivalent band edges strongly influences the carrier heating in these different valleys and consequently the ionization and recombination, too. However, often the experimental data were published without specification of the sample orientation[2,4,6] or the influence of the many-valley band structure was assumed to be negligible,[5] while only in Refs. 1, 3, and 7 was attention paid to this question.

With regard to theoretical considerations, the hot-carrier capture by attractive centers in the model of the Lax cascade with assistance of long-wavelength acoustic phonons[8,9] or high-energy phonons[10] and the impact ionization of shallow centers[11—14] were described for the one-valley case only, which in comparison with experimental results is limited to a symmetric orientation of the heating field with regard to the valleys. The role of intervalley transfer was included into the calculation of the breakdown field for band-band ionization in Ge by Chuenkov,[15] but with an analytic approximation for the distribution function of the electrons.

In the present paper the low-temperature current-voltage behavior in n-type Si is investigated. In Sec. II the experimental procedure is described and those results which will be used for comparison with numerical data are shown. In Sec. III the Monte Carlo calculations are presented taking the many-valley band structure and the relevant interaction processes of the electrons with phonons and impurities into account. In Sec. III A the recombination and ionization coefficients are presented as sums over the contributions of all the valleys. For each

valley an effective electric field strength E_α is introduced and in Sec. III B the intervalley repopulation, the drift velocity, and the distribution function of the electrons are calculated in dependence on E_α. Then in Secs. III C and III D these numerical results are applied to special orientations of electric and magnetic field strengths, respectively.

The Monte Carlo calculations show that the change of carrier concentration with electric field strongly depends on current orientation; it even exhibits N-type characteristics for the $\langle 110 \rangle$ direction and in the presence of a transverse magnetic field an S-type rise of carrier concentration with electric field applied along $\langle 100 \rangle$ is obtained. The threshold field for impact ionization E_c increases when the current direction is turned from $\langle 111 \rangle$ to $\langle 100 \rangle$ in the absence of H, but an essential decrease of E_c for j parallel to $\langle 100 \rangle$ is obtained with strong magnetic fields. The current-voltage characteristics obtained are in good agreement with the experimental results (Sec. IV), especially when the anisotropy of the carrier scattering on acoustic phonons is included.

II. EXPERIMENTAL

The P-doped Si samples were cut in the form of parallelepipeds from (110) disks with the desired crystallographic orientations, i.e., the applied electric field along $\langle 100 \rangle$, $\langle 110 \rangle$, or $\langle 111 \rangle$. The current contacts were alloyed from Sb-doped Au. The investigations were performed in a wide range of doping with donor concentrations between 0.5×10^{14} and 20×10^{14} cm^{-3} and acceptor concentrations between 0.4×10^{13} and 6×10^{13} cm^{-3}; the values were determined by an iterative procedure from Hall and conductivity data. The measurements were performed in liquid neon or hydrogen for the sake of good heat transfer. The electric field was applied in form of square pulses with a repetition rate below 20 cps and a duration down to 1 μsec, the lower limit determined by

the high resistance of the samples at the chosen temperatures and the parasitic capacities. The current-voltage characteristics were obtained by measuring the voltage drop along a resistance in series with the sample and the whole voltage applied to the sample, which includes the contact zones. In the presence of a magnetic field, of course, the electric field is not homogeneous in the sample because the Hall field is shunted by the contact areas, but this distortion was not taken into account.

The current-voltage characteristics split up significantly for $E_p \geq 20$ V/cm for the different orientations with $j\langle 111\rangle > j\langle 110\rangle > j\langle 100\rangle$. While for $\langle 111\rangle$ the current is monotonously rising with increasing E_p for all samples studied, it exhibits a saturation region between 40 and 100 V/cm for both of the other orientations, if N_A is small enough,[16-18] connected either with the appearance of transverse fields on account of broken symmetry of valleys 1 and 2 for $\langle 110\rangle$ or with the repopulation into valley 1 with the heavy effective mass along $\langle 100\rangle$. [Compare Fig. 1—instead of the pair of valleys on one axis, only one valley is presented because they are indistinguishable.] A strong rise of the current density is observed for fields above 200 V/cm in dependence on N_A, determining the low-temperature breakdown, the critical fields being lower for higher concentrations of neutral donors, of course. Experimental results at 27.1 K are shown for the current direction along $\langle 100\rangle$ in Fig. 2.

A transverse magnetic field effects a decrease of the current for weak electric fields caused by the usual magnetoresistivity, but a significant rise for heating electric fields as expected on account of the influence of the created transverse electric fields on carrier repopulation.[17] Experimental results are demonstrated in Fig. 2 for H parallel to $\langle 0\bar{1}1\rangle$, when the resulting Hall field does not change the symmetry of carrier heating in the valleys 2 and 3 (compare Fig. 1). The dependence of the current density on the magnetic field for various fixed values of the applied electric field is depicted in Fig. 3 and exhibits the strong change between 0.25 and 0.6 T and then the transition to a saturation of the influence of H. The represented data were measured after 1-μs pulse duration and it cannot be excluded that for the region of applied fields E_p between 150 and 800 V/cm the current changes with magnetic fields for $H \geq 0$. 4 T are not higher in fact, because the time-dependent increase of the current pulse due to RC during the first μs becomes counterbalanced for longer pulses by a drop of j for these fields, the origin of which is not clear at the present. For applied fields
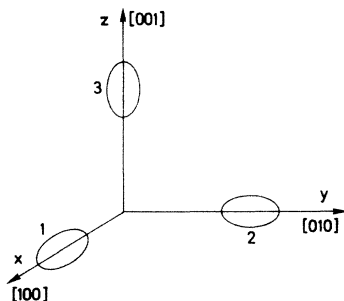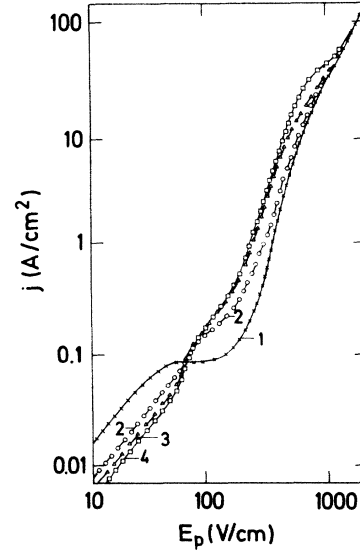

FIG. 2. Current density measured vs applied electric field strength along $\langle 100\rangle$ at 27.1 K in dependence on a transverse magnetic field: curve 1, 0; 2, 0.34; 3, 0.565, and 4, 0.83 T for a sample with $N_D - N_A = 4.4 \times 10^{14}$ and $N_A = 1 \times 10^{13}$ cm^{-3}.

above $E_p = 400$ V/cm the change of the current by the magnetic field becomes diminished as demonstrated by curves 9 and 10 in Fig. 3 and for $E_p \geq 2000$ V/cm there is no influence of H on the current-voltage characteristics to be observed any more.

The angular dependence of j on a transverse magnetic field mirrors the symmetry properties of the regarded current orientation, of course, for weak magnetic fields. It is most pronounced for j along $\langle 111\rangle$, but less for j along $\langle 100\rangle$. For strong magnetic fields it can be neglected in the latter case completely.

III. THEORY

A. Basic approach

The rate equation for the carrier concentration n in dependence on time t and electric field strength E in many-valley semiconductors is similar to the one-valley case when effective rates for recombination B_T^* and for impact ionization A_J^* are introduced. These are the sums of the contributions of the single valleys weighted by the part of the electrons populating the regarded valley,[15,19] while the thermal activation of an electron A_T has the same probability for all valleys and the Auger recombination is assumed to be negligible:

$$\frac{\partial n}{\partial t} = A_T(N_D - N_A - n) - B_T^*(N_A + n)n$$

$$+ A_J^*(N_D - N_A - n)n \ , \tag{1}$$

with

$$B_T^* = \sum_{\alpha=1}^{\lambda} B_{T,\alpha}\frac{n_\alpha}{n} \ , \quad A_J^* = \sum_{\alpha=1}^{\lambda} A_{J,\alpha}\frac{n_\alpha}{n} \ . \tag{2}$$

For the sample doping of interest in the prebreakdown region n can be neglected in comparison to $N_D - N_A$ and N_A.[7]

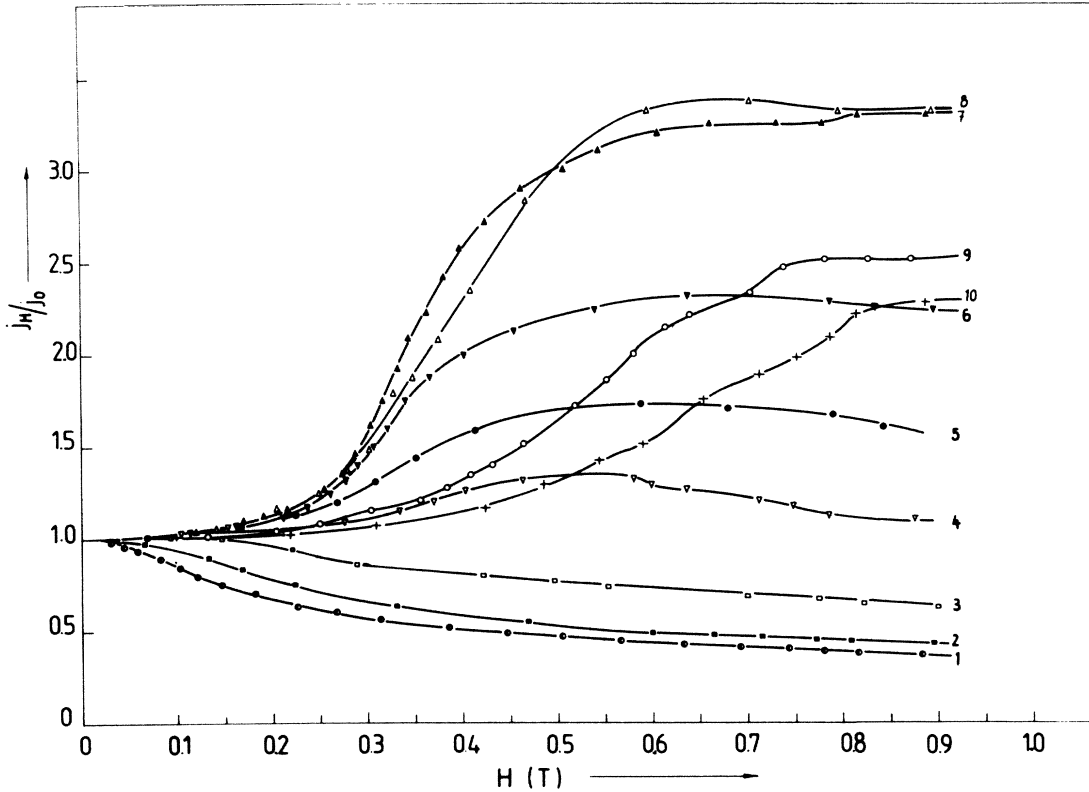FIG. 1. Orientations of axes and valleys for n-type Si.

FIG. 3. Current density along $\langle 100 \rangle$ in dependence on a magnetic field parallel to $\langle 011 \rangle$ with applied electric field as parameter: curve 1, 8; 2, 37; 3, 60; 4, 75; 5, 90; 6, 120; 7, 180; 8, 356; 9, 617; and 10, 782 V/cm for a sample with $N_D - N_A = 4.4 \times 10^{14}$, and $N_A = 1 \times 10^{13}$ cm^{-3}.

The redistribution of the electrons among the valleys is obtained from the intervalley rate equations:[17,20]

$$\frac{\partial(n_\alpha - n/\lambda)}{\partial t} = -\sum_{\beta \neq \alpha} \left[\frac{n_\alpha}{\tau_\alpha} - \frac{n_\beta}{\tau_\beta} \right], \quad \alpha = 1,\ldots,\lambda - 1 \quad (3)$$

with

$$\frac{1}{\tau_\alpha} = \frac{1}{\tau_{f,\alpha}} + \frac{B_{T,\alpha}(N_A + n)}{\lambda} \quad (4)$$

for the probability of an electron of valley α to be scattered into valley $\beta \neq \alpha$ with $1/\tau_{f,\alpha}$ representing the inter-valley scattering (IS) probability on account of absorption and emission of phonons, while the IS on impurities is negligible in comparison to the second term, which describes the probability that the electron leaves the valley α by recombination.[19] The contribution by impact ionization to $1/\tau_\alpha$ is small in comparison with emission of high-energy phonons for doping that is not too strong.[19] The steady-state solution of Eq. (3) yields the well-known relation

$$\frac{n_\alpha}{n} = \frac{\tau_\alpha}{\sum_{\beta=1}^{\lambda} \tau_\beta} . \quad (5)$$

In order to determine the field dependence of n and n_α it is necessary to calculate $A_{J,\alpha}$, $B_{T,\alpha}$, and τ_α as functions of the electric field in each valley. The effective electric and magnetic field strengths in a valley α are obtained by the

Herring-Vogt transformation:[21]

$$E_\alpha = E \left[\frac{m}{m_1} \cos^2\varphi_\alpha + \frac{m}{m_t} \sin^2\varphi_\alpha \right]^{1/2}, \quad (6)$$

$$H_\alpha = H \left[\frac{m}{m_t} \right]^{1/2} \left[\frac{m}{m_t} \cos^2\psi_\alpha + \frac{m}{m_1} \sin^2\psi_\alpha \right]^{1/2}, \quad (7)$$

where φ_α and ψ_α are the angles between the longitudinal axis of the regarded valley and the applied fields $\mathbf{E}$ and $\mathbf{H}$, respectively, and $m = (m_t^2 m_1)^{1/3}$.

The Boltzmann equations for the concerned valleys are solved by the Monte Carlo method (e.g., Refs. 17 and 22), and the dependence of the distribution functions, the IS times on phonons $\tau_{f,\alpha}$, and the components of the mean drift velocity v_α on the effective electric field E_α are found. $B_{T,\alpha}$ and $A_{J,\alpha}$, as functions of the fields are then obtained by

$$B_{T,\alpha} = \frac{\sum_{p} v_\alpha \sigma_T f_{p,\alpha}}{\sum_{p} f_{p,\alpha}}, \quad A_{J,\alpha} = \frac{\sum_{p}' v_\alpha \sigma_J f_{p,\alpha}}{\sum_{p} f_{p,\alpha}} \quad (8)$$

with the cross sections σ_T and σ_J and the prime denoting that the summation is restricted to states $\mathbf{p}$ with an energy ϵ greater than the ionization energy ϵ_J. The energy dependence of σ_T is chosen to be the same as in an isotropic semiconductor[8] due to the above-mentioned Herring-Vogt transformation:

$$\sigma_T = \frac{\sigma_1}{\xi} \int_0^\infty \frac{(\xi+\eta)^2[1-(1+\eta/\gamma)]\exp(-\eta/\gamma)d\eta}{\{[1+(\xi+\eta)/4]^2-\xi\}^3\{1-\exp[-(\xi+\eta)/\gamma]\}}$$

(9)

with $\xi = 2\epsilon/ms^2$ and $\gamma = 2k_B T/ms^2$, where s denotes an effective isotropic sound velocity and σ_1 is fitted to obtain the experimental value of $B_{T,\alpha}$ for $E \rightarrow 0$ at the given temperature [chosen equal to 6×10^{-6} cm^3/s for Si (Refs. 7 and 23)]. The impact-ionization cross section was not chosen to be energy independent as in Refs. 4 and 11–14, but equal to[5]

$$\sigma_J = \sigma_0 \left[\frac{\epsilon}{\epsilon_J}-1\right] \bigg/ \left[\frac{\epsilon}{\epsilon_J}\right]^{1.25},$$

(10)

with σ_0 fitted by 9.6×10^{-14} cm^2.

B. Numerical procedure

The Monte Carlo calculations are performed for n-type Si at 27 K. With regard to the electron-phonon interaction processes the same parameters as in Refs. 24, 17, and 18 are used: g_1 and g_2 phonons for scattering between the valleys on the same axis with $\hbar\omega_{g_1} = 12$ meV and $\hbar\omega_{g_2} = 62$ meV as well as f_1, f_2, and f_3 phonons for scattering between valleys on perpendicular axes with energies of 18, 47, and 59 meV, respectively. Their coupling constants are given by the deformation potentials of 0.65, 7.5, 0.0474, 4.3, and 2 in units of 10^8 eV/cm, respectively. For the chosen lattice temperature these phonons are only weakly excited and, therefore, with exception of the g_1 and f_1 phonons only emission processes are regarded. Concerning the interaction with long-wavelength acoustic phonons after the Herring-Vogt transformation, an effective isotropic sound velocity $s = 9.04\times10^5$ cm/s and an effective deformation potential of 9 eV are used.[25,17] As the ionization energies of shallow donors in Si are about the energy of f_2 phonons, ϵ_J will be approximated by 47 meV.

The total electric field $\mathbf{E}$ is computed for the given values and directions of the applied electric field $\mathbf{E}_p$ and magnetic fields $\mathbf{H}$ taking the arising transverse electric fields into account. It should be remembered, therefore, that not only a change of the angle between $\mathbf{E}_p$ and $\mathbf{H}$ but also of one of the values E_p or H effects a change of the angle between the effective fields $\mathbf{E}_\alpha$ and $\mathbf{H}_\alpha$. In order to simplify the calculations we restrict ourselves to a perpendicular orientation of $\mathbf{E}_p$ and $\mathbf{H}$, which leads to an orthogonality of $\mathbf{E}_\alpha$ and $\mathbf{H}_\alpha$ as a consequence. For numerical calculations values equal to 0.27, 0.6, and 1.3 T were used for H_α, which correspond to applied magnetic fields of 0.353 and 0.775 T along $\langle 001\rangle$. As for classically strong fields, the angular dependence of the transverse magnetic field can be neglected;[26] these parameters are fit to describe the influence of a magnetic field perpendicular to a current directed along $\langle 100\rangle$.

Figure 4 shows the dependence of the out-scattering probability from the α valley $1/\tau_\alpha$, for two different acceptor concentrations and the probabilities $B_{J,\alpha}$ as well as $A_{T,\alpha}$, on E_α with H_α as a parameter, while results for the mean drift velocity in a valley $v_\alpha(E_\alpha)$ were already pub-
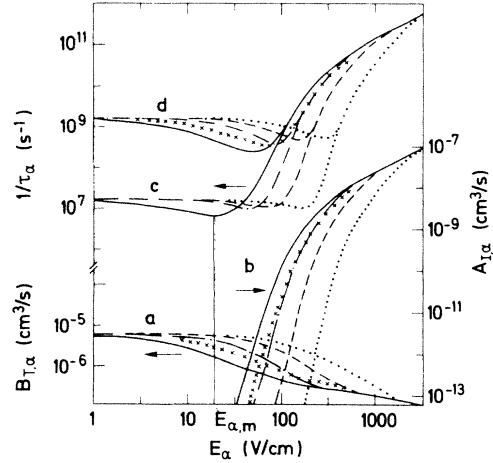

FIG. 4. Coefficients for (a) recombination $B_{T,\alpha}$, (b) impact ionization $A_{J,\alpha}$, (c) and (d) outscattering probability $1/\tau_\alpha$ from the α valley, calculated as functions of the effective electric field E_α for n-type Si at 27 K in dependence on the effective magnetic field H_α: ———, 0; —·—·—·, 0.27; — — —, 0.6; · · · ·, 1.3 T with an acceptor concentration (c) 4×10^{12} and (d) 4×10^{14} cm^{-3}. × (Here and further on the crosses are for the case when the anisotropy of carrier scattering on acoustic phonons is taken into account), the dependences for E_α parallel to the longitudinal valley axes and $H_\alpha = 0$.

lished previously.[17,26] The recombination probability $B_{T,\alpha}$ (curves a in Fig. 4) decreases when E_α increases for fixed H, caused by the growing carrier heating; i.e., the number of electrons with small energy, which are captured with a high probability by the ionized donors, decreases.[27] On the other hand, for fixed F_α the recombination probability increases with growing H_α due to the usual magnetoresistance connected with carrier cooling by the presence of a magnetic field. It should be noticed that fixed E_α incorporate a decrease of the applied electric field when H_α grows.

The ionization probability $A_{J,\alpha}$ (curves b in Fig. 4) increases very sharply with growing E_α because it is sensitive to the distribution function $f_{p,\alpha}$ in the energy range $\epsilon \geq \epsilon_J$, which strongly increases with growing E_α and determines the field dependence of $A_{J,\alpha}$.

The probability of intervalley scattering by emission of f_2 phonons is determined by the same part of the distribution function as $A_{J,\alpha}$ due to $\epsilon_J \approx \hbar\omega_{f_2}$ and differs from $A_{J,\alpha}$ therefore only by a factor independent from E_α as verified in.[19] The emission of f_2 phonons represents the main contribution to $1/\tau_\alpha$ [see Eq. (4)] for the high-field region, while in the low-field region the recombination dominates if the acceptor concentration is not too low (curves d), and already for $N_A = 4\times10^{12}$ cm^{-3} (curves c) the emission of f_1 phonons becomes noticeable too. Therefore, according to the contributions of the main processes represented by curves a and b, the IS probability $1/\tau_\alpha$ exhibits a minimum at $E_{\alpha,m}$. $E_{\alpha,m}$ increases when H_α or N_A increase as can be seen from curves c and d.

C. Numerical results for $H = 0$

Figure 5 shows the dependence of the impact ionization $A_J^*(N_D - N_A)$ and the recombination $B_T^* N_A$ [compare Eq.
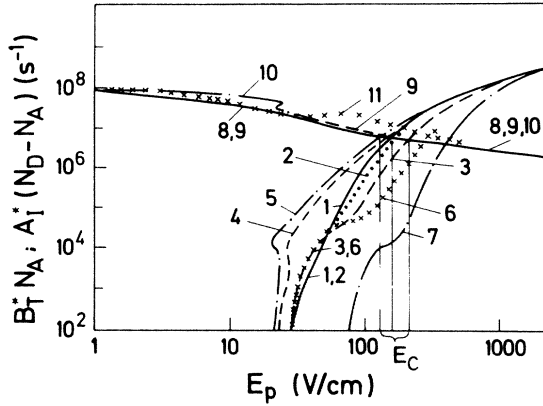
FIG. 5. Probabilities of the impact ionization $A_J^*(N_D-N_A)$ (curves 1–7) and of the recombination $B_T^*N_A$ (curves 8–11) in dependence on applied electric field E_p for $j||\langle 111\rangle$ (curves 1 and 8), $j||\langle 110\rangle$ (curve 2), $j||\langle 100\rangle$ (curves 3–7 and 9–11) at $H=0$ T (curves 1–3, 6, 8, 9, and 11), $H=0.35$ T (curve 4), and $H=0.78$ T (curves 5, 7, and 10) for $N_D-N_A=5.5\times10^{15}$ and $N_A=2\times10^{13}$ cm^{-3}. × (curves 6 and 11) as in Fig. 4; curve 7 shows $A_J^*(N_D-N_A)$ in dependence on the total electric field E (instead of E_p).

(1)] on the applied electric field for $N_D-N_A=5\times10^{15}$ cm^{-3}—results for other values of N_D-N_A are obtained by a parallel shift of the curve, of course—and exhibits the threshold field E_c for breakdown defined usually by the intersection of $B_T^*N_A$ and $A_J^*(N_D-N_A)$, because in the steady-state solution of Eq. (1),

$$n = \frac{A_T(N_D-N_A)}{B_T^*N_A - A_J^*(N_D-N_A)} , \tag{11}$$

the denominator vanishes. Table I represents some examples of E_c for given $N_A/(N_D-N_A)$.

In the prebreakdown region the contribution of the impact ionization to the denominator of Eq. (11) is small and the behavior of the electron concentration as a function of E_p is determined by $1/B_T^*$. Therefore Fig. 6 represents $B_T^*(0)/B_T^*(E_p)$ for current directions along $\langle 111\rangle$, $\langle 110\rangle$, and $\langle 100\rangle$ for $N_D-N_A=5.5\times10^{14}$ cm^{-3} and $N_A=2\times10^{12}$ cm^{-3} (curves 1, 2, and 4, respectively) as well as $N_A=4\times10^{14}$ cm^{-3} (curves 1, 3, and 5, respectively). For the $\langle 111\rangle$ direction only the situation with equal carrier population of all valleys is regarded and since the IS is negligible then, B_T^* and A_J^* do not depend on N_A and we obtain a universal function $n(E_p)$ independent of doping. Note that the solutions in the form of "loops" of transverse fields in a narrow region of applied electric fields because of broken symmetry of the valley populations[28,29,17,18] are not taken into account here.

Concerning the current orientation along $\langle 100\rangle$ the effective field in the first valley is small compared to that of both the others according to Eq. (6) and since $1/\tau_\alpha$ depends on E_α as shown in Fig. 4, an intervalley repopulation arises and changes A_J^* and B_T^* essentially. For $E_\alpha < E_{\alpha,m}$—where the IS probability decreases with rising E_α due to $1/\tau_\alpha \sim B_{T,\alpha}N_A/3$—the cold valley 1 becomes depleted achieving a minimal population value of 23.3% for $N_A=2\times10^{13}$ cm^{-3} (in comparison to 33% for equal valley population) for $E_{p,m}$ as shown by curve 1 in Fig. 7.
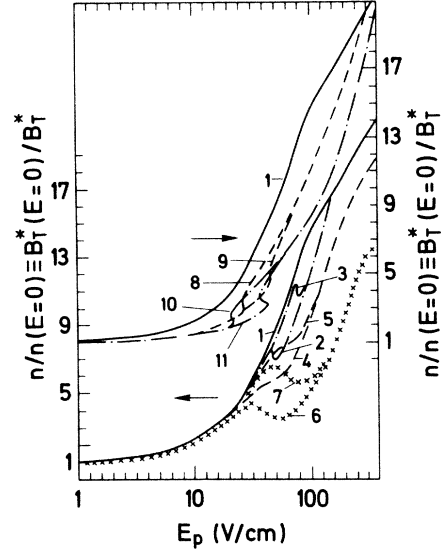

FIG. 6. Normalized electron concentration as a function of E for $j||\langle 111\rangle$ (curve 1), $j||\langle 110\rangle$ (curves 2 and 3), and $j||\langle 100\rangle$ (curves 4–11) at $H=0$ T (curves 1–7), $H=0.35$ T (curves 8 and 9), and $H=0.78$ T (curves 10 and 11) for $N_D-N_A=5.5\times10^{14}$ cm^{-3} with $N_A=2\times10^{12}$ cm^{-3} (curves 1, 2, 4, 6, 8, and 10) and $N_A=4\times10^{14}$ cm^{-3} (curves 1, 3, 5, 7, 9, and 11). In the prebreakdown region n is proportional to $1/B_T^*$. × as in Fig. 4 for the anisotropy of the acoustic phonon scattering taken into account.

The minimal population value and the corresponding $E_{p,m}$ increase when N_A decreases. However, almost all the electrons are transferred into the cold valley 1, if the strongly E_α-dependent phonon-assisted IS becomes the most important process as exhibited by the strong rise of curve 1 in Fig. 7.

Therefore, for $E_p < E_{p,m}$ only the hot valleys contribute to impact ionization because $A_{J,2}=A_{J,3} > A_{J,1}$ on account of the strong dependence on E_α and $E_2/E_1 = E_3/E_1 = (m_1/m_t)^{1/2}$. In this case
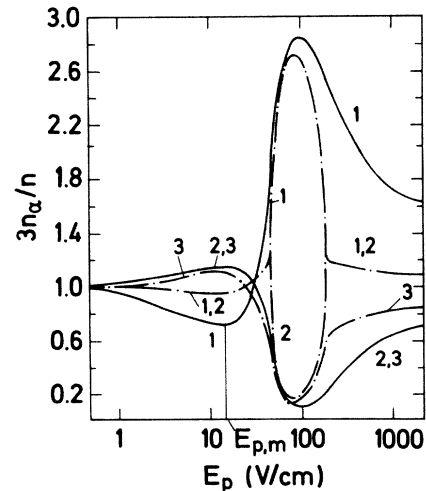

FIG. 7. Relative populations $3n_\alpha/n$ as functions of applied electric field E_p with $N_A=2\times10^{13}$ cm^{-3} for $j||\langle 100\rangle$ (———) and $j||\langle 110\rangle$ (– – – –), for $H=0$ T. Numbers 1,2,3 correspond to $\alpha=1,2,3$.

$$A_J^* = \frac{2A_{J,2}}{B_{T,2} \sum\limits_{\alpha=1}^{\lambda} \frac{1}{B_{T,\alpha}}} \qquad (12)$$

is larger than for j parallel to $\langle 111 \rangle$ because the effective field in the hot valley is larger than the effective field for $\langle 111 \rangle$.

For $E_p > E_{p,m}$, on the other hand, the f_2 phonon emission dominates as mentioned earlier and we obtain $1/\tau_\alpha \sim A_{J,\alpha}$ (compare Fig. 4). Therefore $A_{J,\alpha}\tau_\alpha$ does not depend on α and from Eqs. (2) and (5) it results that the electrons of any valley give the same contribution to the impact ionization, which reads

$$A_J^* = \frac{3}{\sum\limits_{\alpha} \frac{1}{A_{J,\alpha}}} \approx 3A_{J,1} ; \qquad (13)$$

i.e., the field dependence of the cold valley determines the impact-ionization probability, which therefore is reduced in comparison to the value for the $\langle 111 \rangle$ direction due to the different effective fields. A_J^* from Eq. (13) is an order of magnitude smaller than in the case given by Eq. (12) for the same E_p. This implies that A_J^* grows sufficiently slowly with increasing E_p in the vicinity of $E_{p,m}$, where the transition from (12) to (13) takes place. For $N_A = 2 \times 10^{13}$ cm^{-3} this transition is exhibited by curve 3 in Fig. 5. The electric field, for which this transition occurs, is shifted to higher E_p when N_A increases in accordance with the shift of $E_{p,m}$ in Fig. 7.

For the high-electric-field region $1/\tau_\alpha$ and $A_{J,\alpha}$ vary more smoothly with E_α and the intervalley redistribution decreases with further increase of E_p, as exhibited by the solid lines in Fig. 7. The contribution of the hot valleys to the denominator in Eqs. (5) or (13) is not negligible any longer and A_J^* tends towards the value of the $\langle 111 \rangle$ direction.

With regard to the $\langle 110 \rangle$ current direction some new features originate from the multivalued electron distribution[24,17,18] when in a certain region of the applied field the electrons predominantly populate only one of the valleys 1 or 2 as indicated by the dot-dashed curves in Fig. 7. This valley becomes the coldest one because a transverse electric field is created on account of the broken symmetry of the population of valleys 1 and 2. Therefore the dependence of A_J on E_p for $\langle 110 \rangle$ lies between the values for $\langle 111 \rangle$ and $\langle 100 \rangle$, as can be seen from curve 2 in Fig. 5.

Concerning the recombination process the dependence of $1/B_T^*$ on E_p can be seen from Fig. 6 for the prebreakdown region. While for the $\langle 111 \rangle$ direction curve 1

demonstrates a smooth increase, peculiarities are again present for both the other directions. For the current along $\langle 100 \rangle$ we obtain from Eqs. (2) and (5) that the electrons of all three valleys equally contribute to B_T^* and

$$\frac{1}{B_T^*} = \frac{1}{3} \sum_\alpha \frac{1}{B_{T,\alpha}} , \qquad (14)$$

showing that the field dependence is dominated by the hot valley, for which $1/B_{T,\alpha}$ is the largest term. However, the cold valleys also give some contribution because $B_{T,\alpha}$ does not vary as strongly with E_α as $A_{J,\alpha}$ does.

For the region with $E_p > E_{p,m}$ we obtain

$$B_T^* = B_{T,1} \qquad (15)$$

since, for valley 1 as the coldest valley τ_1 is sufficiently greater than $\tau_{2,3}$. Because $1/B_T^*$ from Eq. (15) is smaller than a value from Eq. (14) for the same E_p there is a flat transition region in the vicinity of $E_{p,m}$. Consequently, $1/B_T^*$ for $\langle 100 \rangle$ is more slowly increasing with E_p in this transition region than for $\langle 111 \rangle$, as depicted by curves 4 and 5 in comparison to curve 1 in Fig. 6. For the $\langle 110 \rangle$ direction as already discussed in connection with A_J^* the multivalued electron distribution in a certain region of field strength effects a very strong repopulation among valleys 1 and 2 (dash-dotted curves in Fig. 7) and leads to an N-type behavior of $B_T^*(0)/B_T^*(E_p)$, as exhibited by curves 2 and 3 in Fig. 6.

Due to the considerable reduction of impact ionization and the slight increase of recombination on account of intervalley transfer, the threshold field for impact ionization E_c increases when the current orientation is turned from $\langle 111 \rangle$ to $\langle 100 \rangle$ (see Table I). Figure 8 shows the current-voltage characteristics. Already for weak electric fields the current density for $\langle 100 \rangle$ is slightly higher than for $\langle 111 \rangle$ because of the electron repopulation into the hot valleys with larger mobility (compare Fig. 7) due to recombination. With growing field strength the redistribution into the cold valleys due to phonon-assisted IS effects N-type negative differential conductivity (NDC) as expected,[28] but it is shifted towards higher currents in comparison to the earlier calculations which neglected the change of carrier concentration with applied field strength. Similar to the preceding results of Fig. 6 for the current, these values for the orientation along $\langle 110 \rangle$ are also between those for $\langle 111 \rangle$ and $\langle 100 \rangle$.

D. Results for $j||\langle 100 \rangle$ and strong transverse H

In order to discuss the influence of a transverse magnetic field the new results are presented in the same figures

TABLE I. Impact-ionization threshold field E_c (V/cm) in dependence on current orientation and magnetic field for various concentrations of acceptors (cm^{-3}) and of neutral donors $N_D - N_A$ (cm^{-3}).

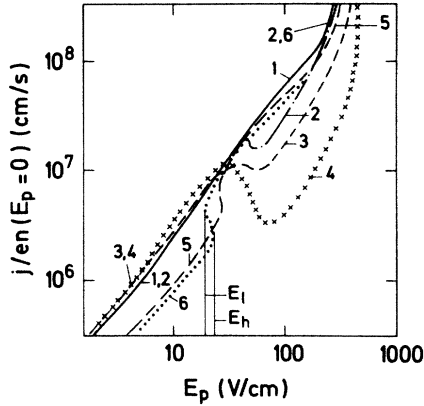| $N_A = N_D^+$	4×10^{12}	4×10^{12}	4×10^{12}	2×10^{13}
$N_D - N_A$	5.5×10^{13}	5.5×10^{14}	5.5×10^{15}	5.5×10^{14}
$j||\langle 111 \rangle$, $H = 0$ T	534	187	100	364
$j||\langle 110 \rangle$, $H = 0$ T	548	192	118	375
$j||\langle 100 \rangle$, $H = 0$ T	687	259	154	490
$j||\langle 100 \rangle$, $H = 0.35$ T	623	199	89	414
$j||\langle 100 \rangle$, $H = 0.78$ T	554	188	81	373

FIG. 8. Calculated current-voltage characteristics in n-type Si at 27 K for $j||\langle 111 \rangle$ (curve 1), $j||\langle 110 \rangle$ (curve 2), $j||\langle 100 \rangle$ for $H = 0$ T (curves 3 and 4) and for $H = 0.35$ T (curve 5) as well as for 0.78 T (curve 6). $N_D - N_A = 5.5 \times 10^{14}$ and $N_A = 2 \times 10^{13}$ cm^{-3}. $\times$ as in Fig. 4 for $H = 0$ T.

as the numerical data for the absence of H. First of all, it is immediately to be seen that A_J^* as well as B_T^* (Fig. 5), and consequently n (Fig. 6) and j (Fig. 8), become S-type functions of the applied electric field E_p. Of course their dependences on the total electric field strength E remain qualitatively the same as before due to the contribution of the Hall field E_H to the total field. This is demonstrated, for instance, with regard to $A_J^*(N_D - N_A)$ in Fig. 5, which is shown for $H = 0.78$ T as a function of E_p by curve 5, and of E by curve 7. Curve 7, in turn, obviously differs from curve 3 for $H = 0$ only by a shift to higher fields and a more pronounced change of the slope. The pronounced "kink" is caused by the very rapid carrier transfer from the valley 1 (see Fig. 1) to the others in the presence of high magnetic fields. Valley 1 has become the hot one because H_1 is small and E_1 is large due to Eqs. (7) and (6). On account of this intervalley repopulation the ratio of the transverse field E_H to the applied one increases superlinear with E as depicted by curve 2 in Fig. 9. This means, on the other hand, that an increase of E is even possible for diminishing E_p because of the strong
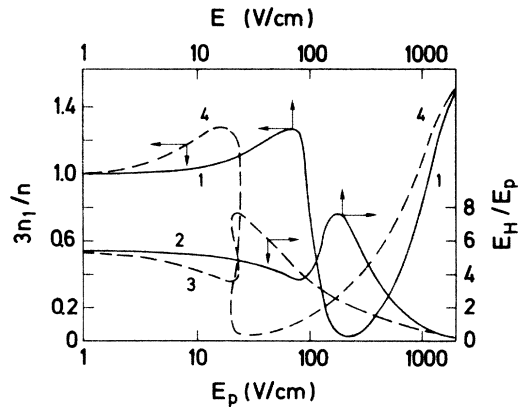

FIG. 9. Dependence of the relative population of the first valley $3n_1/n$ (curves 1 and 4) and of the ratio of the transverse electric field E_H to the applied electric field E_p (curves 2 and 3) on the total electric field E (curves 1 and 2) and on E_p (curves 3 and 4) for $j||\langle 100 \rangle$ and $H = 0.78$ T.

growth of E_H. Therefore E_H/E_p as a function of E_p shows an S-type behavior, as exhibited by curve 3 in Fig. 9, and causes the S-type dependence on E_p of the intervalley repopulation (curve 4 in Fig. 9) and, consequently, of A_J^* (curves 4 and 5 in Fig. 5), $1/B_T^*$, or n, (curves 8–11 in Fig. 6), as well as j (curves 5 and 6 in Fig. 8). For $E_p > 30$ V/cm the current in the strong magnetic field (in this region there is already almost no difference between the influence of $H = 0.35$ and 0 T) is considerably greater than for $H = 0$ (curve 3). This is caused by the electron transfer from valley 1 into both the others, which have a high mobility along $\langle 100 \rangle$ in the presence of H instead of the repopulation in its absence into valley 1, which has a small mobility along the current direction.

The most essential influence of the magnetic field is obtained for the impact-ionization probability (Fig. 5), which increases more than 2 orders of magnitude when H increases from 0 to 0.8 T for weak electric fields. This increase of A_J^* diminishes for growing E_p, but it can still be observed for 200 V/cm. The difference between $A_J^*(0)$ and $A_J^*(H)$ results from the contribution of E_H to the effective field in the valley [Eq. (6)]. The low-energy electrons are not heated more strongly in spite of an increase of E_H because H declines them from the direction of E, but the high-energy electrons are heated more strongly in the presence of H because the magnetic field has almost no influence on their trajectories due to the high scattering probabilities of these electrons when $\epsilon > 35$ meV for 0.8 T or $\epsilon > 8$ meV for 0.35 T.[30] But these high-energy electrons are important for impact ionization and they are the reason why, at $H = 0.8$ T, the impact ionization for the current along the $\langle 100 \rangle$ direction succeeds the value of A_J for $\langle 111 \rangle$ in the absence of H. The threshold field E_c decreases therefore with the magnetic field, as shown in Table I.

IV. DISCUSSION OF THE RESULTS

The calculated current-voltage characteristics are in good agreement with the experimentally obtained results. With regard to the dependence on the orientation of the current a correct presentation is consequently obtained with $j_{\langle 111 \rangle} > j_{\langle 110 \rangle} > j_{\langle 100 \rangle}$ and $E_{c\langle 111 \rangle} < E_{c\langle 110 \rangle} < E_{c\langle 100 \rangle}$. Quantitatively, the region with N-type ndc for $\langle 100 \rangle$, which determines the lower part of the field region with current saturation observed in our long-time measurements on account of the formation of domains with high static electric fields,[31] exhibits the correct field strength with respect to the lower field limit, but does not extend up to values comparable with the experimental data and curve 3 of Fig. 8 therefore exhibits a rise of the current density at too-low applied fields and a less-pronounced difference between $j_{\langle 111 \rangle}$ and $j_{\langle 100 \rangle}$ in the prebreakdown region. When anisotropy of the carrier scattering on acoustic phonons[32] is taken into account, however, the Monte Carlo calculations yield[30,33] that the mean velocity and particularly the phonon-assisted IS probability, as well as the impact ionization, decrease compared to the data for an effective isotropic scattering if the effective field E_α is directed along the longitudinal axis of the valley α at $H = 0$. On the other hand, these entities slightly

increase if E_α coincides with a transverse axis of the valley. This difference is caused by the greater interaction probability with acoustic phonons when the electron is moving along the longitudinal axis of the valley with the weaker heating. The results obtained when the anisotropy is included into the Monte Carlo calculations are indicated by crosses in all the figures.

The dependence of the concentration on E_p even exhibits an N-type behavior as can be seen from curves 6 and 7 in Fig. 6 for two different acceptor concentrations. This circumstance effects a more pronounced ndc of course, as exhibited in Fig. 8 for $N_A = 2 \times 10^{13}$ cm^{-3}, and the diminished carrier concentration in the high-field region consequently shifts the breakdown field E_c for $\langle 100 \rangle$ towards higher values. The field range with current saturation as well as the breakdown field agree with the numerical data obtained.

In the presence of the strong magnetic fields the current-voltage characteristics in the high electric field region[30] and consequently the breakdown fields are almost unchanged if the anisotropy of carrier scattering on the acoustic phonons is taken into account, but a severe influence is observed in the range of S-type ndc. The lower field limit E_1 for S-type ndc (indicated in Fig. 8) is shifted to lower values while the upper field limit E_h is shifted

to higher ones; for instance, for $H = 0.8$ T, E_1 is changed from 23.3 to 18.7 V/cm and E_h from 27.3 to 35 V/cm.

In comparison to the experimental results all essential features agree well: the decrease of the current in the weak-applied-field region due to the usual magnetoresistance and a decrease of the electron concentration in the presence of H (compare Fig. 6); the steep rise on account of ndc; and the shift of the breakdown field to smaller values. As already mentioned in Sec. II the measurements included the sample regions near the contacts and the data were not corrected with respect to the distortion of the field. Therefore instead of an abrupt jump of the current density at constant electric field expected for S-type characteristics only a steep rise is observed.[31]

For the current direction along $\langle 111 \rangle$ the current is again diminished by transverse magnetic fields for weak electric fields E_p both experimentally and numerically, but there is practically no influence of transverse magnetic fields on the breakdown field E_c.

ACKNOWLEDGMENTS

*On leave from the Institute of Semiconductors of the Academy of Sciences of the Ukrainian S.S.R., Kiev, U.S.S.R.

[1]S. N. Koenig, R. D. Brown, and W. Schillinger; Phys. Rev. 128, 1668 (1962).

[2]E. I. Zavarizkaya, Fiz. Tverd. Tela (Leningrad) 6, 3545 (1964).

[3]Yu. A. Astrov and A. A. Kastalskii, Fiz. Tekh. Poluprovod. 5, 1257 (1971) [Sov. Phys.—Semicond. 5, 1111 (1971)].

[4]J. F. Palmier, Phys. Rev. B 6, 4557 (1972).

[5]V. F. Bannaya, L. I. Veselova, E. M. Gershenson, and V. A. Chuenkov, Fiz. Tekh. Poluprov. 7, 1972 (1973) [Sov. Phys.—Semicond. 7, 1315 (1974)].

[6]J. C. Sohm, J. Phys. Chem. Solids 18, 181 (1961).

[7]M. Asche, H. Kostial, and O. G. Sarbey, Phys. Status Solidi B 91, 521 (1979).

[8]V. N. Abakumov and I. N. Yassievich, Zh. Eksp. Teor. Fiz. 71, 657 (1976) [Sov. Phys.—JETP 44, 345 (1976)].

[9]V. N. Abakumov, V. I. Perel, and I. N. Yassievich, Fiz. Tekh. Poluprov. 12, 3 (1978) [Sov. Phys.—Semicond. 12, 1 (1978)].

[10]M. Asche and O. G. Sarbey, Pis'ma Zh. Eksp. Teor. Fiz. 28, 625 (1978) [JETP Lett. 28, 578 (1978)].

[11]J. Yamashita, J. Phys. Soc. Jpn. 16, 720 (1961).

[12]A. Zylberstejn, Phys. Rev. 127, 744 (1962).

[13]W. Pickin, Phys. Rev. B 20, 2451 (1979).

[14]F. A. Khan and D. P. Bhattacharya, J. Phys. C 17, 3463 (1984).

[15]V. A. Chuenkov, Fiz. Tekh. Poluprov. 11, 1055 (1977) [Sov. Phys.—Semicond. 11, 629 (1977)].

[16]M. Asche and H. Kostial, Phys. Status Solidi B 93, K89 (1979).

[17]M. Asche, Z. S. Gribnikov, V. V. Mitin, and O. G. Sarbey, Goryachie Elektrony v Mnogodolinikh Poluprovodnikakh (Naukova dumka, Kiev, 1982).

[18]M. Asche, Multivalued Distributions of Hot Electrons between Equivalent Valleys, Vol. 58 of Topics in Applied Physics, edited by L. Reggiani (Springer, Berlin, 1985), p. 149.

[19]V. V. Mitin, Appl. Phys. C (to be published).

[20]Z. S. Gribnikov and V. V. Mitin, Phys. Status Solidi B 68, 153 (1975).

[21]C. Herring and E. Vogt, Phys. Rev. 101, 944 (1956).

[22]L. Reggiani, General Theory, Vol. 58 of Topics in Applied Physics, edited by L. Reggiani (Springer, Berlin, 1985), p. 7.

[23]P. Norton, T. Braggins, and H. Levinstein, Phys. Rev. Lett. 30, 488 (1973).

[24]M. Asche, Z. S. Gribnikov, V. M. Ivashchenko, H. Kostial, V. V. Mitin, and O. G. Sarbey, Zh. Eksp. Teor. Fiz. 81, 1347 (1981) [Sov. Phys.—JETP 54, 715 (1981)].

[25]C. Canali, C. Jacoboni, F. Nava, G. Ottaviani, and A. Alberigi-Quaranta, Phys. Rev. B 12, 2265 (1975).

[26]V. M. Ivastchenko and V. V. Mitin, Ukr. Fiz. Zh. 29, 123 (1984).

[27]V. N. Abakumov, L. N. Kreshchuk, and I. N. Yassievich, Fiz. Tekh. Poluprov. 12, 264 (1978) [Sov. Phys.—Semicond. 12, 152 (1978)].

[28]M. Asche, Z. S. Gribnikov, V. M. Ivashchenko, H. Kostial, and V. V. Mitin, Phys. Status Solidi B 114, 429 (1982).

[29]M. Asche and H. Kostial, Phys. Status Solidi B 120, K83 (1983).

[30]V. V. Mitin, Z. Phys. (to be published).

[31]O. G. Sarbey, L. F. Kurtenok, E. A. Movchan, V. V. Mitin, and M. Asche, Proceedings of the 14th International Conference on the Physics of Semiconductors, Edinburg, 1978, edited by B. L. H. Wilson (Institute of Physics, Bristol, 1979), p. 339.

[32]M. H. Jørgensen, N. O. Gram, and N. I. Meyer, Solid State Commun. 10, 337 (1972).

[33]V. M. Ivashchenko and V. V. Mitin, Fiz. Tekh. Poluprov. 19, 5 (1985).